Investigation of new particle formation at the summit of Mt. Tai, China

Ganglin Lv[1], Xiao Sui[1], Jianmin Chen[1,2*], Rohan Jayaratne[3], Abdelwahid Mellouki[1,4]

[1]School of Environmental Science and Engineering, Environment Research Institute, Shandong University, Jinan, Shandong 250100, China

[2]Shanghai Key Laboratory of Atmospheric Particle Pollution and Prevention (LAP3), Institute of Atmospheric Sciences, Fudan University, Shanghai 200433, China

[3]International Laboratory for Air Quality and Health, Science and Engineering Faculty, Queensland University of Technology, GPO Box 2434, Brisbane QLD 4001, Australia

[4]Institut de Combustion, Aérothermique, Réactivité et Environnement, CNRS, 45071 Orléans cedex 02, France

Correspondence to: Jianmin Chen (jmchen@fudan.edu.cn); Tel.: +86 53188363711; fax: +86 531 88361990

Abstract. To date few field observations of new particle formation (NPF) have been carried out at the high-elevation mountain sites in China. Simultaneous measurements of particle size distributions, gas species, meteorological conditions, mass concentration and chemical composition of $PM_{2.5}$ were performed at the summit of Mt. Tai (1534 m ASL) from 25 July to 24 August 2014 (I), 21 September to 9 December 2014 (II), and 16 June to 7 August 2015 (III), to investigate the NPF characteristics related to the relatively clean mountain-top environment. The NPF events were identified based on particle size distributions, and 66 such events were observed in a period of 164 days - corresponding to an occurrence frequency of 40 %. Formation rates of 3 nm (J_3) and growth rates (GR) were in the range of 0.82-25.04 cm^{-3} s^{-1} and 0.58-7.76 nm h^{-1}, respectively. On the average, the condensation sink (CS), O_3 concentration, temperature and relative humidity (RH) were lower, whereas the SO_2 concentration was higher on NPF days than on non-NPF days. The onset of NPF events at the summit of Mt. Tai might not be limited by the initial sulfuric acid concentration because of the approximate sulfuric acid proxy concentrations in the early morning on NPF days and non-NPF days. The analysis of back trajectory indicated that the majority of transport pathways on NPF days came from the northwest, and the air masses going through the polluted areas could increase the occurrence of NPF. Four NPF events, with the potential elevated $PM_{2.5}$ and trace gases concentrations, were observed during hazy episodes. As a case study on 11 November 2014, the NPF event might be driven by enhanced solar radiation at noon and the changing air mass transport with the rich precursor concentrations.

Keywords. New particle formation; Mountain observation; Favourable conditions; Hazy episodes

1 Introduction

Atmospheric aerosols play a critical role in affecting global radiation balance and climate, directly through scattering and absorption of solar radiation, and indirectly by modifying cloud properties as potential cloud condensation nuclei (CCN) (Kuang et al., 2010). Aerosol particles are involved in several atmospheric chemistry processes such as enhancing haze and

decreasing visibility, and they can also harm human health by inhalation (Han, 2012). Previous studies have showed that the nucleation of atmospheric gas-phase precursors and the subsequent growth to larger particles, widely known as new particle formation (NPF), is the largest source of atmospheric aerosol particles (Zhang et al., 2012). Field observations have exhibited that NPF typically increase the particle number concentration by a factor between two and ten (Gong et al., 2010). Model studies also revealed that NPF accounted for 5-50 % of CCN in the lower boundary layer (Spracklen et al., 2008). An in-depth study of the process of NPF and its effects could help control atmospheric aerosol pollution in China.

With the development of instruments that measure particle size distribution, NPF events have been widely observed all over the world in recent decades. These observation sites included northern-most sub-arctic, remote boreal forests, industrialized agricultural regions, high-iodine coastal environments, and polluted urban areas (Dal Maso et al., 2002). The frequency of NPF events varies significantly between locations. Hallar et al. (2011) reported that NPF events in urban areas such as Pittsburgh occurred on about 35-50 % of all days, while remote background sites in Finland and Sweden only showed such events on 2-27 % of days. Manninen et al. (2010) found that the frequency of NPF days ranged from 21 % to 57 % based on the observations at twelve field sites around Europe, and the number of observed NPF days was closely related to the regional atmospheric conditions.

In the past decade, many campaigns and studies on NPF have been carried out in China. In 2004 Wiedensohler et al. (2004) first reported the observation of NPF events in China using a Twin Differential Mobility Particle Sizer (TDMPS). Soon after, Liu et al. (2008) made observations of NPF at a rural/coastal site in XinKen (Guangdong Province). In 2005, Gao et al. (2009) investigated the occurrence of NPF in a suburban environment in the Yangtze River delta using a Wide-range Particle Spectrometer (WPS). Thereafter, several observations of the NPF have been reported in urban/suburban/rural environments around China (An et al., 2015; Wang et al., 2011). However, there have not been many observations of NPF on mountain-top sites in China so far. Zhang et al. (2016) reported the occurrence of NPF on Mt. Huang (1840 m ASL) with the WPS instrument from April to July 2008. However, these results had significant limitation in measurement methods and seasonal variation. It is clear that multi-season observations using nanometer-scale instruments would be essential and valuable for the NPF research in mountain environments.

Previous researches have shown that sulfuric acid, ammonia, organic vapors, and iodide species in the atmosphere were involved in nucleation process in specific conditions. Gaseous sulfuric acid was the most critical candidate that participated in binary, ternary and ion induced nucleation (Boy et al., 2005; Wang et al., 2011; Zhang, 2010; Saunders et al., 2010; Allan et al., 2015). It has also been shown that the nucleation rate is a function of sulfuric acid concentration with a power dependency exponent, whose value of exponent varies significantly between different nucleation theories (Kulmala et al., 2006; Wang et al., 2011). However, the occurrence of NPF cannot be determined by a single sulfuric acid factor, and other factors such as pre-existing particles, trace gases, meteorological conditions, and air mass transport should also be considered. However, comprehensive investigations of these factors affecting the occurrence of NPF in China are mainly

conducted in urban/suburban/rural environments. Since the mechanism of NPF under the heavily polluted conditions has significant difference to that under the relatively clean conditions, the intensive and comprehensive investigation of NPF on mountain-top sites may be very important.

Particle formation and growth rates vary with field environments. Kulmala et al. (2004) reviewing a number of studies found that the typical formation rate was in the range of 0.01-10 cm^{-3} s^{-1}. In urban areas it may be about 100 cm^{-3} s^{-1}, while in coastal zones it can be as high as 10^4-10^5 cm^{-3} s^{-1}. Typical growth rate of newly formed particles ranges from 1 to 20 nm h^{-1}, and at some coastal areas it is as high as 200 nm h^{-1}.

In this paper, we present the results of the intensive field campaigns at the summit of Mt. Tai (1534 m ASL) related to the relatively clean mountain-top environment. This study was based on simultaneous measurements of particle size distributions, meteorological conditions, gaseous species, mass concentration and chemical composition of $PM_{2.5}$ during three campaigns (25 July to 24 August 2014, I; 21 September to 9 December 2014, II; 16 June to 7 August 2015, III). The general characteristics of the NPF events were calculated on the basis of particle size distributions, and factors affecting NPF occurrence were discussed by analyzing condensation sink (CS), sulfuric acid, trace gas concentrations and meteorological parameters. In addition, one typical NPF event was specifically investigated to further explore the unusual NPF occurrence during hazy episodes.

2 Methodology

2.1 Site description

The observation was conducted at the summit of Mt. Tai (36.25 °N, 117.1 °E, 1534 m ASL), located in the middle part of Shandong Province, eastern China. Mt. Tai is one of the highest mountains near the East China Sea on the transport path of the Asian continental outflow (Li et al., 2011), adjacent to the Bohai Sea (B-S) and Yellow Sea (Y-S). The field site is nearly at the summit of Mt. Tai, and its surroundings are dominated by dense vegetation and mountains with few anthropogenic sources. The nearest small city, Tai'an (population: 670,000), is located about 15 km away to the south and southeast. The city of Ji'nan (population: 2,800,000), capital of Shandong Province, is 60 km to the north. During daytime, elevation of Mt. Tai reaches close to the top of the planetary boundary layer (PBL) and the site is therefore representative of the region (Zhang et al., 2014; Sun et al., 2016). All the instruments were installed inside a large container, sampling through short inlet tubes from the container at a height of about 3 m above the ground level.

2.2 Measurement techniques

Two types of size distribution instruments, namely neutral cluster and air ion spectrometer (NAIS) and wide-range particle spectrometer (WPS), two gas monitors (SO_2 and O_3), an instrument for mass concentration of $PM_{2.5}$ and a monitor for chemical composition in $PM_{2.5}$ were used in this study. In addition, meteorological parameters including air temperature (T),

relative humidity (RH), wind speed (WS), wind direction (WD) and visibility were also recorded in real time.

The NAIS is a multichannel nanometer aerosol instrument which can measure the distribution of aerosol particles and ions (charged particles and cluster ions) of both polarities simultaneously. The aerosol particle distribution of NAIS is in the size range of 2-40 nm, and the ion distribution is in the electric mobility range of 0.0013-3.2 $cm^2\ V^{-1}\ s^{-1}$ (equivalent to particle Millikan diameters of 0.8-40 nm). The instrument consists of two multichannel electrical mobility analyzer columns, one for each polarity. The aerosols are classified according to mobility and measured with an array of twenty-one electrometers per column. In this study, the total time of each measurement cycle was set at 5 min, comparing sampling intervals as follows: particles 120 s, ions 120 s and offset 60 s.

The WPS is a high-resolution aerosol spectrometer which combines a differential mobility analyzer (DMA), a condensation particle counter (CPC) and a laser light scattering (LPS). The diameter range of the WPS was from 10 to 10,000 nm, and 48 channels were used in the DMA and 24 channels were used for the LPS. The one scan time for the entire size range was set to 5 min.

The concentration of SO_2 in the atmosphere was measured using a pulsed ultraviolet fluorescence analyzer (Model 43C, Thermo Electron Corporation-TEC), and O_3 was measured using an ultraviolet photometric analyzer (Model 49C, TEC). Mass concentration of $PM_{2.5}$ was detected by a monitor utilizing a combination of beta attenuation and light scattering technology (Model 5030 SHARP Monitor, Thermo Fisher Scientific), and chemical composition in $PM_{2.5}$ was measured by Monitor for Aerosols and Gases (MARGA, ADI20801, Applikon-ECN, Netherlands). Besides, meteorological data were obtained from an automatic meteorological station (MILOS520, Vaisala, Finland).

2.3 Data analysis

2.3.1 Formation rate, growth rate and condensation sink

In this study, particles in the size range of 3-20 nm was regarded as nucleation particles, and the formation rate of nucleation mode particles, $J_{3\text{-}20}$, can be expressed (Dal Maso et al., 2005) as:

$$J_{3\text{-}20} = \frac{dN_{3\text{-}20}}{dt} + F_{\text{CoagS}} + F_{\text{growth}} \quad (1)$$

where $dN_{3\text{-}20}/dt$ is the net rate of increased nucleation mode particles, F_{CoagS} is the coagulation loss and F_{growth} is the loss of particles growing out of size range. In our observation, the F_{growth} term could be neglected because particles growing beyond 20 nm before formation ended was relatively rare. In addition, the formation rate of 3 nm particles, J_3, was also calculated from the NAIS data (Sihto et al., 2006; Kulmala et al., 2012) using the equation:

$$J_3 = \frac{dN_{3\text{-}6}}{dt} + \text{CoagS}_{Dp=4\text{ nm}} \cdot N_{3\text{-}6} + \frac{1}{3\text{ nm}}\text{GR}_{3\text{-}6} \cdot N_{3\text{-}6} \quad (2)$$

Here $\text{CoagS}_{DP=4\text{ nm}}$ represents the coagulation sink of 4 nm particles, an approximation for the interval of 3-6 nm. $GR_{3\text{-}6}$ and $N_{3\text{-}6}$ denote the growth rate and particle number concentration between 3 and 6 nm, respectively.

The particle growth rate, GR, was determined by the maximum concentration method (Kulmala et al., 2012), that is:

$$GR = \frac{\Delta D_m}{\Delta t} = \frac{D_{m2} - D_{m1}}{t_2 - t_1} \quad (3)$$

where D_{m1} and D_{m2} are the geometric median diameter of representative particles at the start time t_1 and the end time t_2, respectively.

Condensation sink, CS, determines the rate of molecules condensing on the pre-existing aerosols, and it is given by (Dal Maso et al., 2005; Kulmala et al., 2001):

$$CS = 2\pi D \sum_i \beta_{Mi} Dp_i N_i \quad (4)$$

where D is the diffusion coefficient for sulfuric acid, and β_M is the size-dependent transitional correction factor.

2.3.2 Sulfuric acid proxy

Direct measurement of gas-phase sulfuric acid wasn't available in this study. Instead, the predictive proxy for sulfuric acid ($[H_2SO_4]$) could be estimated based on solar radiation, SO_2 concentration, CS and RH (Mikkonen et al., 2011):

$$[H_2SO_4] = 8.21 \cdot 10^{-3} \cdot k \cdot SR \cdot [SO_2]^{0.62} \cdot (CS \cdot RH)^{-0.13} \quad (5)$$

Here k is temperature-dependent reaction rate constant, and solar radiation is estimated from Hybrid Single Particle Lagrangian Integrated Trajectory (HYSPLIT) Model in Air Resources Laboratory. The absolute values of solar radiation from HYSPLIT may involve some error with the real solar radiation in the atmosphere, but its diurnal variation pattern is believable.

3 Results and discussion

3.1 Classification and characteristics of the NPF events

Basically, a NPF event could be defined as a distinct burst of new nucleation mode particles and subsequent growth of particles to larger size over a period of time (Dal Maso et al., 2005; Hallar et al., 2011; Wang et al., 2014a; Xiao et al., 2015). For the Mt. Tai observation in this study, neutral particles generally accounted for more than 95 % of the total particles during NPF events, so a detailed discussion of ions will not be included in this paper.

In this study, three campaigns (25 July to 24 August 2014, I; 21 September to 9 December 2014, II; 16 June to 7 August 2015, III) were conducted at the summit of Mt. Tai. For the valid observations of 164 days, the NPF events occurred on 66 days, corresponding to an occurrence frequency of 40 %. NPF events were observed in every month, and the frequent occurrence of NPF was in the campaign II which showed the frequency of 56 % (the others were only 21 % by contrast). The different results could be attributed to the rainy/foggy phenomena in the campaign I and III which hindered the NPF. In this study, we defined the observed start time of the NPF events based on the significant enhancement of the $N_{3\text{-}6}$. As the result, approximately 95 % of the NPF events were initiated at 8:00-11:00 LT (local time) at the summit of Mt. Tai, in agreement

with the previous reports in China (Guo et al., 2012; An et al., 2015; Kulmala et al., 2016; Hao et al., 2015). Previous researches explained that this time period corresponded to intensive photochemical activities, leading to potential precursors for the NPF (Hallar et al., 2011; Guo et al., 2012). Table 1 lists the calculated parameters of all the NPF events observed at the summit of Mt. Tai, such as formation rate of nucleation mode particles, formation rate of 3 nm particles, growth rate, condensation sink, mean sulfuric acid proxy concentration in the early morning (generally 6:00-9:00 LT on Mt. Tai), SO_2 concentration (6:00-13:00 LT), and O_3 concentration (6:00-13:00 LT). Table 2 summarizes the mean, median, 25th percentile, 75th percentile, minimum and maximum of these parameters on the basis of the Table 1. In Table 3, it is also exhibited the characteristics comparison between Mt. Tai and some other typical recent researches in China.

The net increase rates and formation rates of nucleation mode particles on Mt. Tai were in the range of 0.96-48.52 cm^{-3} s^{-1} and 1.10-57.43 cm^{-3} s^{-1}, respectively. Coagulation loss averagely accounted for 24.6 % of the nucleation mode particle formation. The maximal values of the net increase rate and formation rate were in the same day, and the SO_2 concentration also reached the maximum of 12.9±9.6 ppb on 3 December 2014. The formation rates J_3 varied from 0.82 to 25.04 cm^{-3} s^{-1}, and the median, 25th percentile and 75th percentile were 6.15, 3.31 and 9.41 cm^{-3} s^{-1}, respectively. On 3 December 2014, J_3 also peaked, showing an obvious sulfuric acid-controlling NPF event. As shown in Table 3, formation rate at the summit of Mt. Tai was significantly larger than 0.97-10.2 cm^{-3} s^{-1} at the waist of Mt. Tai Mo Shan and 0.09-0.30 cm^{-3} s^{-1} on the top of Mt. Huang (Guo et al., 2012; Zhang et al., 2016), but smaller than the results in Beijing and Shanghai (Xiao et al., 2015; Wang et al., 2015). In addition, the observed formation rate on Mt. Tai was a little larger than the rural/suburban environments in Table 3 (Liu et al., 2008; Yue et al., 2013; Qi et al., 2015), which was likely related to the intensive precursor transport in region (eastern China) and enhanced photochemical activities at the summit of Mt. Tai.

Growth rates $GR_{3\text{-}20}$ at the summit of Mt. Tai ranged from 0.58 to 7.76 nm h^{-1}, and the median, 25th percentile and 75th percentile were 1.55, 1.15 and 2.51 nm h^{-1}, respectively. Growth rate on Mt. Tai was comparable with some mountain observations such as 1.5-8.4 nm h^{-1} at Mt. Tai Mo Shan, 1.42-4.53 nm h^{-1} on Mt. Huang, and 0.8-3.2 nm h^{-1} on Mt. Daban (Du et al., 2015; Guo et al., 2012; Hao et al., 2015; Zhang et al., 2016). Growth rates observed at the rural/suburban/urban sites behaved lager than these mountain observations shown in Table 3 (Yue et al., 2013; Liu et al., 2008; Gao et al., 2011; Qi et al., 2015; Xiao et al., 2015), suggesting that the relatively clean mountain environments might be insufficient vapors for newly formed particle growth.

3.2 Factors affecting the occurrence of NPF

Favorable condition of NPF events varies in the different environments. In order to further explore the factors affecting the occurrence of NPF at the summit of Mt. Tai, multiple parameters were compared between NPF days and non-NPF days. Figure 1 shows the average diurnal variations of the condensation sink, sulfuric acid proxy, sulfur dioxide, ozone, temperature, and relative humidity during NPF days and non-NPF days over all the campaigns.

3.2.1 Effects of condensation sink and sulfuric acid on the NPF

In principle, the observed NPF events could be considered as the result of competing between sink and source. Newly formed particles are easily scavenged by larger pre-existing particles, leading to the newly formed particles continually being reduced. On the other hand, sufficient low volatility vapors can contribute to persistent nucleation. Therefore, CS and precursor vapors are the key controlling factors associated with the NPF events. As expected, the lower CS and higher precursor concentrations would be favorable for the occurrence of NPF events, similar results shown in Wang et al. (2011) and Guo et al. (2012). In fact, one of them may be the major factor for NPF occurrence because of inter-competition between sink and source. Kanawade et al. (2014) reported that the NPF was not limited for the CS by reason of the approximate values between NPF days and non-NPF days in a semi-rural location, India. In some urban cities of China such as Qingdao, the NPF events could be observed with both of high particle loadings and precursors (Zhu et al., 2014; Kulmala et al., 2016; Xiao et al., 2015).

The hourly average CS on non-NPF days was always higher than that on NPF days (Fig. 1a), corresponding to the daily average values of $2.0 \pm 0.5 \times 10^{-2}$ s^{-1} and $1.4 \pm 0.5 \times 10^{-2}$ s^{-1}, respectively. The result indicates that the occurrence of NPF events at the summit of Mt. Tai might be limited by the lower CS condition. The general diurnal tendencies of the CS on NPF days and non-NPF days were consistent, showing the trough in the morning and the peak in the late afternoon (or at night). The hourly difference values between NPF days and non-NPF days might be decreased after 14:00 LT, such as minimal values between 18:00-20:00 LT, because of new particle formation and subsequent growth. The CS on NPF days varied from 0.1×10^{-2}-28.4×10^{-2} s^{-1}, corresponding median, 25th percentile and 75th percentile were 0.9×10^{-2} s^{-1}, 0.5×10^{-2} s^{-1} and 1.7×10^{-2} s^{-1}, respectively. The result was much larger than 0.5×10^{-3}-3.5×10^{-3} s^{-1} in Hyytiälä, Finland (Dal Maso et al., 2005), but significantly lower than many reports in China such as 0.6×10^{-2}-8.4×10^{-2} s^{-1} in Beijing, 0.9×10^{-2}-3.9×10^{-2} s^{-1} in Nanjing, 0.9×10^{-2}-5.3×10^{-2} in Qingdao, and 1.0×10^{-2}-6.2×10^{-2} s^{-1} in Hong Kong (Zhang et al., 2011; Gao et al., 2012; Guo et al., 2012; An et al., 2015; Herrmann et al., 2014; Zhu et al., 2014). Overall, the environment at the summit of Mt. Tai is relatively clean with the low particle loadings.

Gas-phase sulfuric acid has been identified as an important precursor for nucleation process. Direct emission for sulfuric acid at the summit of Mt. Tai is negligible, and thus the photochemical reactions of SO_2 are the significant source for sulfuric acid in the atmosphere. In this study, the mean sulfuric acid proxy concentrations (6:00-9:00 LT) of all the NPF days were in the range of 0.52×10^6-25.7×10^6 cm^{-3}. Both curves for sulfuric acid proxy concentration peaked at noon (Fig. 1b), which was consistent with the peak time of solar radiation. The maximum hourly average sulfuric acid proxy concentration on NPF days (5.9×10^7 cm^{-3}) was about 60 % higher than that on non-NPF days (3.7×10^7 cm^{-3}), which indirectly reflected an intensive solar radiation on NPF days. In the early morning, the average sulfuric acid proxy concentration on NPF days was 5.23×10^6 cm^{-3}, comparable with 4.1×10^6 cm^{-3} in Beijing but much lower than 2.3×10^7-6.4×10^7 cm^{-3} in Shanghai and

6.6×10^7-7.8×10^7cm^{-3} in Nanjing (Wang et al., 2014b; Wang et al., 2015; Xiao et al., 2015). The polluted observation environments with the elevated sink might require more condensable vapors involving in nucleation, in agreement with the fact that many oversea studies observed less sulfuric acid concentration for the NPF (Dal Maso et al., 2005; Boy et al., 2005). Apart from other precursor species, lower initial sulfuric acid proxy concentration can be partly explained by the relatively lower CS at the summit of Mt. Tai.

The relationships between sulfuric acid, CS and the $N_{3\text{-}6}$ in the early morning are shown in Fig.2. Most of the CS on non-NPF days was situated in the intermediate region (~1.0×10^{-2} s^{-1}), whereas approximately 80 % of the CS on NPF days was less than 1.0×10^{-2} s^{-1}. Expectedly, the left region (small CS) was believed to be more favorable for nucleation than the right region (large CS). The spot distributions on sulfuric acid proxy concentration (Y axis) had no remarkable difference between NPF days and non-NPF days, which was consistent with the tendencies in Fig. 1b (6:00-9:00 LT). This phenomenon might be explained that the intensive photochemical activities frequently occurred because of the enhanced solar radiation and high oxidation capacity at the summit of Mt. Tai in the morning, which leaded to the sufficient vapors for nucleation burst. Therefore, we can conclude that the sulfuric acid concentration sometimes may be not the major limiting factor for the onset of NPF at the summit of Mt. Tai if the estimation for gas-phase sulfuric acid had the high confidence level.

It was noteworthy that the $N_{3\text{-}6}$ showed a significant correlation with the sulfuric acid proxy concentration on NPF days (Fig. 2a). Lots of $N_{3\text{-}6}$ were less than 500 cm^{-3} when the sulfuric acid proxy concentration (Y axis) was lower than 1.0×10^6 cm^{-3}, whereas the $N_{3\text{-}6}$ reached nearly even more than 800 cm^{-3} when the sulfuric acid proxy concentration (Y axis) exceeded 1.0×10^6 cm^{-3}. Further investigation found that sulfuric acid proxy concentration indeed behaved a positive correlation with the $N_{3\text{-}6}$ on many NPF days. In contrast, Fig.2b didn't exhibit similar correlation between the $N_{3\text{-}6}$ and the sulfuric acid proxy concentration on non-NPF days, and the colors ($N_{3\text{-}6}$) were almost evenly distributed on sulfuric acid proxy (Y axis).

As the vital nucleation precursor, sulfuric acid was associated with the freshly nucleation particles. As above, the positive correlation between the sulfuric acid proxy concentration and $N_{3\text{-}6}$ at the summit of Mt. Tai was in accordance with the earlier reports (Kulmala et al., 2006; Wang et al., 2011; Guo et al., 2012). As an example on 14 October 2014 in Fig. 3, the $N_{3\text{-}6}$ reflected a best correlation (R^2 =0.975) with sulfuric acid proxy concentration during NPF event (6:00-14:00 LT). After 14:00 LT, the exceptionally high SO_2 concentrations (change from 2.6 ppb at 14:00 LT to 19.1 ppb at 15:00 LT) resulted in the divarication of them. In principle, the increase of sulfuric acid concentration should be earlier than the $N_{3\text{-}6}$. However, there were some NPF days with zero or negative time delay in this study, such as nearly zero time delay on 14 October 2014 in Fig. 3. Wang et al. (2011) explained that the fore-formed nucleation mode particles and rapid particle growth might account for such zero or negative time delay.

3.2.2 Effects of sulfuric dioxide and ozone on the NPF

As shown in Fig. 1c, almost all the hourly average SO_2 concentrations on NPF days were higher than the corresponding values on non-NPF days (except for the slightly lower values at 1:00 LT and 3:00 LT). The average SO_2 concentrations between 6:00-13:00 LT on NPF days and non-NPF days were 3.2 ppb and 2.6 ppb, respectively, which indicated that the NPF was indeed favorable to the high SO_2 concentration. Photochemical reactions of SO_2 are the major source for sulfuric acid at the summit of Mt. Tai, thus the higher SO_2 concentration can increase the possibility of rich precursors for NPF. In Fig.4, it was noteworthy that the temperature suddenly dropped from 1.3 ℃ to -9.4 ℃ on 30 November 2014. After several days, the exceptionally high SO_2 concentration was observed (7.1±7.2 ppb) at the summit of Mt. Tai (marked in violet block), and frequent NPF events occurred during this period. Reasons for above phenomena might be the anthropogenic pollutants (such as SO_2) from the coal or biomass burning in the upwind region (Li et al., 2015a; Li et al., 2015b).

Some of the NPF events might be lack of sensitivity with SO_2 concentration. On 21 September 2014, for instance, non-NPF event occurred under simultaneously high SO_2 concentration (9.7±7.0 ppb, 6:00-13:00 LT) and CS ($4.0\pm1.2\times10^{-2}$ s^{-1}, 6:00-13:00 LT) conditions. The sink might dominate the inter-competition between sink and source on this day, which possibly limited the nucleation as the some previous reports (Song et al., 2010; Guo et al., 2012; Meng et al., 2015). Therefore, species accompanying with SO_2 emission, such as aerosol particles, were taken account in the investigation of NPF and SO_2. Of course, the coupling of SO_2 and the accompanying species at the summit of Mt. Tai might be weakened a lot during air mass transport.

O_3 has been considered to quantify the oxidation capacity and photochemical activities in the atmosphere, directly reacting with related species such as VOCs and indirectly affecting sulfuric acid formation via hydroxyl and hydroperoxy radicals (Berndt et al., 2010; Gómez Martín et al., 2013; Sorribas et al., 2015; Guo et al., 2012). The daily average O_3 concentrations on NPF days and non-NPF days were 40 ppb and 47 ppb, respectively. Previous reports showed that elevated O_3 concentration was benefit to the occurrence of NPF (An et al., 2015; Guo et al., 2012; Zhang et al., 2016; Huang et al., 2016), but an opposite result was unexpectedly observed in the study. All the hourly average O_3 concentrations on NPF days were lower than that on non-NPF days in Fig. 1d. As we all know, O_3 is usually contributed by anthropogenic emissions on the ground. The different result in the study might be partly explained that the positive rising of O_3 photolysis couldn't offset the negative influence of other pollutants (accompanying with O_3, such as particles). The diurnal variation of O_3 on NPF days showed a small trough in the early morning and the broad peak in the afternoon. The small trough was near the sunset, which might suggest that residual O_3 in the atmosphere was consumed and sulfuric acid was possibly formed during this period. Another remarkable feature was that the hourly difference values of O_3 between NPF days and non-NPF days (Fig. 1d) decreased after 10:00 LT. The decreasing difference values indirectly reflect the intensive solar radiation on NPF days because of the association between O_3 production and solar radiation.

3.2.3 Effects of meteorological conditions on the NPF

Favorable meteorological conditions can promote the occurrence of NPF when precursors are insufficient in the atmosphere (Song et al., 2010). In this study, approximately 90 % of the NPF events occurred on the clear or partial cloudy daytime, suggesting an association between solar radiation and NPF as above. The temperature of all the NPF days varied from -11.8 to 22.1 ℃, and the diurnal temperature showed a cyclic variation with solar radiation. The hourly average temperature on non-NPF days (10.7±1.1 ℃) were always higher than that on NPF days (7.0±1.8 ℃) in Fig. 1e, in agreement with the studies at Mt. Tai Mo Shan and Mt. Huang, China (Guo et al., 2012; Zhang et al., 2016), and in PUY, France (Rose et al., 2015). Guo et al. (2012) indicated that the lower temperature could enhance the nucleation of sulfuric acid and water vapor. Young et al. (2007) explained that effects of lower temperature on the NPF might be related to the atmospheric vertical convection. Anyway, the occurrence of NPF at the summit of Mt. Tai seemed to favor the lower temperature condition.

The RH of all the NPF days ranged from 22 % to 95 %, and diurnal RH behaved inversely correlated with the solar radiation. The hourly average RH on NPF days (63±5 %) was much lower than the corresponding value on non-NPF days (88±2 %) in Fig. 1f, and the maximum difference value between two curves was about 30 %. Anti-correlation between the NPF and RH can be identified at the summit of Mt. Tai, similar to the results in Beijing, Nanjing, Hong Kong, and Mt. Huang (An et al., 2015; Wang et al., 2014a; Shen et al., 2016; Zhang et al., 2016; Guo et al., 2012). The actual role of RH on the NPF still has controversies so far. Hamed et al. (2011) indicated that the RH affected the source of the NPF via decreasing solar radiation under the high RH condition. In addition, increasing CS (sink) under the high RH condition has also been suggested to explain the negative effect of RH (Hamed et al., 2011; Guo et al., 2012).

A wide range of wind speed was on NPF days at the summit of Mt. Tai, varying from 0.2 m s^{-1} to 7.8 m s^{-1}. Compared with non-NPF days, the wind direction on NPF days had a narrow range in west-southwest (250 º-300 º) and east-southeast (85 º-110 º) (Fig. 5a). These directions corresponded to an elevated SO_2 concentration, especially in the wind directions between 270 ºto 300 º. This suggests that the gas point sources from the above two directions can increase the probability of the NPF occurrence in a certain extent. The accumulation mode particles showed a high level of concentration when the wind came from the northeast (30 º-90 º), which could, at least partly, explain the less occurrence of NPF from the northeast direction. The nucleation and Aitken modes particles were almost evenly distributed in each wind direction if there was not the NPF event, indicating that there were few local particle sources for the nucleation and Aitken modes particles around the observation site.

To characterize the origins of air masses, air mass backward trajectories for 72 h at 6:00 LT at 1535 m ASL were simulated using the HYSPLIT model developed by the National Oceanic and Atmospheric Administration (NOAA) Air Resources Laboratory. Figure 6a illustrates the air mass backward trajectories of all the NPF days, and Fig. 6b is for all the non-NPF days.

The air mass backward trajectories were mainly classified into three categories: continental air masses, local air masses and maritime air masses. The majority of transport pathways during NPF days were continental air masses, which accounted

for 80 % of the total air masses. Continental air masses on NPF days mainly came from the northwest direction, and they largely originated from Siberia and passed over Mongolia, Inner Mongolia, Shanxi Province, Hebei Province, and Beijing with the long movements. Four-fifths of the continental air masses on NPF days passed though the polluted areas (Beijing, Hebei Province, Shanxi Province, Henan Province, and Shaanxi Province) before reaching the observation site. In contrast, only two-fifths of continental air masses on non-NPF days passed though above polluted areas, and the others were either coming from the south (cleaner part of China) or transporting over Bohai Sea (B-S) and Yellow Sea (Y-S). It seems plausible that air masses going through polluted areas could increase the occurrence of NPF, because transported air masses brought high level of anthropogenic precursors from the polluted areas. In addition, the local and maritime backward trajectories on NPF days accounted for 8 % and 12 % of the total trajectories, respectively (local air masses were 12 % and maritime air masses were 25 % on all non-NPF days). The local air masses were mainly from surroundings such as Jinan, Nanjing, Zhengzhou with short pathways, whereas the maritime air masses originated over the Bohai Sea, Yellow Sea and East China Sea (E-S). Comparison between the Fig. 6a and Fig. 6b found that there were less proportion of maritime air masses and shorter routes over ocean areas on NPF days, suggesting that maritime air masses might not be the favorable conditions for the occurrence of NPF at the summit of Mt. Tai.

3.3 Typical NPF events during hazy episodes

In Sect. 3.2, it mainly investigated the favorable conditions for the occurrence of NPF at the summit of Mt. Tai. In fact, the NPF events could also be observed under some specific conditions, such as hazy episodes. According to the Chinese Meteorological Administration, the hazy episode can be identified when the atmospheric visibility is less than 10 km and the RH is less than 80 % simultaneously. In the atmosphere, hazy episodes are always accompanied with elevated $PM_{2.5}$ concentrations. The higher $PM_{2.5}$ concentration may mean increased particle loadings, which suppresses the nucleation to a great extent. Indeed, the hourly average $PM_{2.5}$ concentrations on non-NPF days (~26 μg m^{-3}, 6:00-9:00 LT) were always higher than the corresponding values on NPF days (~20 μg m^{-3}, 6:00-9:00 LT) before 9:00 LT. Therefore, an intensive investigation of NPF events occurring during hazy episodes (named as NPF hazy events below) is very important.

In this study, four NPF hazy events (26 July 2014, 17 October 2014, 18 October 2014, and 11 November 2014) were observed during the three campaigns, and the related parameters on four days (named as NPF hazy days below) were shown in Table 4. The $PM_{2.5}$ concentrations on NPF hazy days were significantly higher than the average of all NPF days observed at the summit of Mt. Tai, but potential high precursor concentrations might exist simultaneously because of the high level of SO_2, O_3 and CO concentrations. The temperature and RH were in accordance with the corresponding climates, but wind speed of the each NPF hazy day varied a lot. It was noteworthy that the start time of NPF hazy events was around noon, an obvious time delay compared with the general start time of 8:00-11:00 LT (seen in Set. 3.1). This phenomenon might suggest that the enhanced solar radiation at noon could be an important factor for the NPF hazy events. In order to further

explore the characteristics of NPF hazy events, one NPF event on 11 November 2014 was selected for case study. The time series of the particle size distribution, meteorological parameters, trace gases, chemical composition and mass concentration of $PM_{2.5}$ are illustrated in Fig. 7.

On 11 November 2014, the NPF event was clearly observed at about 11:30 LT. The visibility of this day was always in a low level, and fog episode dispersed with the RH decreasing. It had been hazy episode before the NPF event occurred, and thus the day was considered as NPF hazy day. The highest temperature was about 7 ℃ and lowest RH was 66 % at noon. At about 10:00 LT, the obvious increase in SO_2 concentration (Fig. 7d), decrease in $PM_{2.5}$ concentration and change in chemical composition of $PM_{2.5}$ (Fig. 7e) were observed simultaneously. The observation site is located on the mountain top without any stationary source nearby, and above changes therefore may suggest that there was another polluted air mass transported to observation site, contributing to the NPF to a certain extent. The average mass concentrations of sulfate, ammonium, nitrate, OC and EC were 4.1, 4.6, 4.1, 7.6 and 0.7 μg m^{-3} during 6:00-9:00 LT, respectively. In contrast, their average concentrations were 13.1, 11.2, 11.1, 10.0 and 0.2 μg m^{-3} in order during 11:00-18:00 LT. The ratio of sulfate increased a lot before and after 10:00 LT, suggesting that the new air mass might be S (SO_2)-rich.

Air mass backward trajectories for 72 h at 1535 m ASL at 14:00, 12:00, 10:00, 8:00 and 6:00 LT on 11 November 2014 are shown in Fig.8. Fig.8 illustrated that the origin of transported air mass moved from eastern China (Jiangsu and Anhui Provinces, line A and B) to western China (line C, D and E) at about 10:00 LT, in agreement with above analysis in Fig. 7. The latter air mass backward trajectories (line C, D and E) passed through the heavily polluted areas, such as Shanxi and Shaanxi Provinces, before reaching the observation site, leading to the potential increase of precursor concentrations.

4. Conclusions

Field observations of the NPF at the mountain-top sites are scarce in China and its related researches could significantly contribute to atmospheric aerosol pollution control. A comprehensive investigation of the NPF was conducted at the summit of Mt. Tai (1534 m ASL), eastern China, from 25 July to 24 August 2014 (I), 21 September to 9 December 2014 (II) and 16 June to 7 August 2015 (III), using two types of size distribution instruments (NAIS and WPS) and including two trace gases, multiple meteorological parameters, mass concentration and chemical composition of $PM_{2.5}$. During the 164 days, 66 NPF events were identified based on the particle size distributions, giving an occurrence frequency of 40 %. Most of the NPF events were initiated at about 8:00-11:00 LT, in agreement with the intensive photochemical activities. The J_3, $J_{3\text{-}20}$ and growth rates were in the range of 0.82-25.04 cm^{-3} s^{-1}, 1.10-57.43 cm^{-3} s^{-1} and 0.58-7.76 nm h^{-1}, respectively. In comparison with other studies in China, J_3 at the summit of Mt. Tai was slightly larger than some rural/suburban environments, which probably was associated with the intensive air mass transport in eastern China and enhanced solar radiation at the summit of Mt. Tai. Instead, growth rates showed the lower values compared with some rural/suburban/urban environments of China,

suggesting insufficient vapors related to growth rate on Mt. Tai.

The CS on NPF days at the summit of Mt. Tai was 0.1×10^{-2}-28.4×10^{-2} s^{-1}, much lower than other urban reports in China. The NPF events were in favor to occur in lower CS, O_3 concentration, temperature and RH conditions, whereas the elevated SO_2 concentration was observed on NPF days. Without consideration the errors of solar radiation, the average sulfuric acid proxy concentration (6:00-9:00 LT) on NPF days ranged from 0.52×10^6 cm^{-3} to 25.7×10^6 cm^{-3}. The role of sulfuric acid concentration on the NPF onset might be uncertain because of no evident superiority in sulfuric acid proxy concentration on NPF days in the early morning. The NPF events were more common when the wind was from the west-southwest and east-southeast directions. The majority of air mass backward trajectories on NPF days came from the northwest, and the air masses going through the polluted areas can increase the occurrence of NPF at the summit of Mt. Tai.

Four NPF events were observed during hazy episodes, and their delayed start time might imply that the enhanced solar radiation at noon made an important role on the occurrence of NPF hazy events. Elevated $PM_{2.5}$ and trace gases concentrations might be observed on NPF hazy days. As a case study on 11 November 2014, the NPF might be caused by enhanced solar radiation at noon and changing air mass transport which brought the potential high precursor concentration.

Acknowledgements. This work was supported by National Natural Science Foundation of China (No. 41375126), Mount Tai Scholar Grand (ts20120552), Cyrus Tang Foundation (No.CTF-FD2014001), Ministry of Science and Technology of China (SQ2016ZY01002231, 2014BAC22B01), and Marie Skłodowska-Curie Actions (H2020-MSCA-RISE-2015-690958).

References

Allan, J. D., Williams, P. I., Najera, J., Whitehead, J. D., Flynn, M. J., Taylor, J. W., Liu, D., Darbyshire, E., Carpenter, L. J., Chance, R., Andrews, S. J., Hackenberg, S. C., and McFiggans, G.: Iodine observed in new particle formation events in the Arctic atmosphere during ACCACIA, Atmos. Chem. Phys., 15, 5599-5609, doi:10.5194/acp-15-5599-2015, 2015.

An, J., Wang, H., Shen, L., Zhu, B., Zou, J., Gao, J., and Kang, H.: Characteristics of new particle formation events in Nanjing, China: Effect of water-soluble ions, Atmos. Environ., 108, 32-40, doi:10.1016/j.atmosenv.2015.01.038, 2015.

Berndt, T., Stratmann, F., Sipilä, M., Vanhanen, J., Petäjä, T., Mikkilä, J., Grüner, A., Spindler, G., Lee Mauldin Iii, R., Curtius, J., Kulmala, M., and Heintzenberg, J.: Laboratory study on new particle formation from the reaction OH + SO_2 : influence of experimental conditions, H_2O vapour, NH_3 and the amine tert-butylamine on the overall process, Atmos. Chem. Phys., 10, 7101-7116, doi:10.5194/acp-10-7101-2010, 2010.

Boy, M., Kulmala, M., Ruuskanen, T. M., Pihlatie, M., Reissell, A., Aalto, P. P., Keronen, P., Dal Maso, M., Hellen, H., Hakola, H., Jansson, R., Hanke, M., and Arnold, F.: Sulphuric acid closure and contribution to nucleation mode particle growth, Atmos. Chem. Phys., 5, 863-878, doi:10.5194/acp-5-863-2005, 2005.

Dal Maso, M., Kulmala, M., Lehtinen, K. E. J., Mäkelä, J. M., Aalto, P., and O'Dowd, D.: Condensation and coagulation sinks and formation of nucleation mode particles in coastal and boreal forest boundary layers, J. Geophys. Res., 107, 8097, doi:10.1029/2001JD001053, 2002.

Dal Maso, M., Kulmala, M., Riipinen, I., Wagner, R., Hussein, T., Aalto, P. P., and Lehtinen, K. E. J.: Formation and growth of fresh atmospheric aerosols : Eight Years of Aerosol Size Distribution Data from SMEAR II, Hyytiälä, Finland, Boreal Environ. Res., 10, 323-336, 2005.

Du, W., Sun, Y. L., Xu, Y. S., Jiang, Q., Wang, Q. Q., Yang, W., Wang, F., Bai, Z. P., Zhao, X. D., and Yang, Y. C.: Chemical characterization of submicron aerosol and particle growth events at a national background site (3295 m a.s.l.) in the Tibetan Plateau, Atmos. Chem. Phys., 15, 10811-10824, doi:10.5194/acp-15-10811-2015, 2015.

Gómez Martín, J. C., Gálvez, O., Baeza-Romero, M. T., Ingham, T., Plane, J. M., and Blitz, M. A.: On the mechanism of iodine oxide particle formation, Phys. Chem. Chem. Phys., 15, 15612-15622, doi:10.1039/c3cp51217g, 2013.

Gao, J., Wang, T., Zhou, X., Wu, W., and Wang, W.: Measurement of aerosol number size distributions in the Yangtze River delta in China: Formation and growth of particles under polluted conditions, Atmos. Environ., 43, 829-836, doi:10.1016/j.atmosenv.2008.10.046, 2009.

Gao, J., Chai, F., Wang, T., and Wang, W.: Particle number size distribution and new particle formation (NPF) in Lanzhou, Western China, Particuology, 9, 611-618, doi:10.1016/j.partic.2011.06.008, 2011.

Gao, J., Chai, F., Wang, T., Wang, S., and Wang, W.: Particle number size distribution and new particle formation: New characteristics during the special pollution control period in Beijing, J. Environ. Sci., 24, 14-21, doi:10.1016/s1001-0742(11)60725-0, 2012.

Gong, Y., Hu, M., Cheng, Y., Su, H., Yue, D., Liu, F., Wiedensohler, A., Wang, Z., Kalesse, H., and Liu, S.: Competition of coagulation sink and source rate: New particle formation in the Pearl River Delta of China, Atmos. Environ., 44, 3278-3285, doi:10.1016/j.atmosenv.2010.05.049, 2010.

Guo, H., Wang, D. W., Cheung, K., Ling, Z. H., Chan, C. K., and Yao, X. H.: Observation of aerosol size distribution and new particle formation at a mountain site in subtropical Hong Kong, Atmos. Chem. Phys., 12, 9923-9939, doi:10.5194/acp-12-9923-2012, 2012.

Hallar, A. G., Lowenthal, D. H., Chirokova, G., Borys, R. D., and Wiedinmyer, C.: Persistent daily new particle formation at a mountain-top location, Atmos. Environ., 45, 4111-4115, doi:10.1016/j.atmosenv.2011.04.044, 2011.

Hamed, A., Korhonen, H., Sihto, S.-L., Joutsensaari, J., Järvinen, H., Petäjä, T., Arnold, F., Nieminen, T., Kulmala, M., Smith, J. N., Lehtinen, K. E. J., and Laaksonen, A.: The role of relative humidity in continental new particle formation, J. Geophys. Res., 116, doi:10.1029/2010jd014186, 2011.

Han, S.: Effect of Aerosols on Visibility and Radiation in Spring 2009 in Tianjin, China, Aerosol Air Qual. Res., 12, 211-217, doi:10.4209/aaqr.2011.05.0073, 2012.

Hao, J., Yin, Y., Li, X., Yuan, L., and Xiao, H.: Observations of Nucleation Mode Particles Formation and Growth on Mount Huang, China, Procedia Engineering, 102, 1167-1176, doi:10.1016/j.proeng.2015.01.242, 2015.

Herrmann, E., Ding, A. J., Kerminen, V. M., Petäjä, T., Yang, X. Q., Sun, J. N., Qi, X. M., Manninen, H., Hakala, J., Nieminen, T., Aalto, P. P., Kulmala, M., and Fu, C. B.: Aerosols and nucleation in eastern China: first insights from the new SORPES-NJU station, Atmos. Chem. Phys., 14, 2169-2183, doi:10.5194/acp-14-2169-2014, 2014.

Huang, X., Zhou, L., Ding, A., Qi, X., Nie, W., Wang, M., Chi, X., Petäjä, T., Kerminen, V.-M., Roldin, P., Rusanen, A., Kulmala, M., and Boy, M.: Comprehensive modelling study on observed new particle formation at the SORPES station in Nanjing, China, Atmos. Chem. Phys., 16, 2477-2492, doi:10.5194/acp-16-2477-2016, 2016.

Kanawade, V. P., Shika, S., Pöhlker, C., Rose, D., Suman, M. N. S., Gadhavi, H., Kumar, A., Nagendra, S. M. S., Ravikrishna, R., Yu, H., Sahu, L. K., Jayaraman, A., Andreae, M. O., Pöschl, U., and Gunthe, S. S.: Infrequent occurrence of new particle formation at a semi-rural location, Gadanki, in tropical Southern India, Atmos. Environ., 94, 264-273, doi:10.1016/j.atmosenv.2014.05.046, 2014.

Kuang, C., Riipinen, I., Sihto, S. L., Kulmala, M., McCormick, A. V., and McMurry, P. H.: An improved criterion for new particle formation in diverse atmospheric environments, Atmos. Chem. Phys., 10, 8469-8480, doi:10.5194/acp-10-8469-2010, 2010.

Kulmala, M., Dal Maso, M., Mäkelä, M., Pirjola, L., Väkevä, M., Aalto, P., Miikkulainen, P., and Hämeri, K.: On the formation, growth and composition of nucleation mode particles, Tellus B, 53, 479-490, doi:10.1034/j.1600-0889.2001.d01-33.x, 2001.

Kulmala, M., Vehkamäki, H., Petäjä, T., Dal Maso, M., Lauri, A., Kerminen, V. M., Birmili, W., and McMurry, P. H.: Formation and growth rates of ultrafine atmospheric particles: a review of observations, J. Aerosol Sci., 35, 143-176, doi:10.1016/j.jaerosci.2003.10.003, 2004.

Kulmala, M., Lehtinen, K. E. J., and Laaksonen, A.: Cluster activation theory as an explanation of the linear dependence

between formation rate of 3 nm particles and sulphuric acid concentration, Atmos. Chem. Phys., 6, 787-793, doi:10.5194/acp-6-787-2006, 2006.

Kulmala, M., Petäjä, T., Nieminen, T., Sipila, M., Manninen, H. E., Lehtipalo, K., Dal Maso, M., Aalto, P. P., Junninen, H., Paasonen, P., Riipinen, I., Lehtinen, K. E., Laaksonen, A., and Kerminen, V. M.: Measurement of the nucleation of atmospheric aerosol particles, Nat. Protoc., 7, 1651-1667, doi:10.1038/nprot.2012.091, 2012.

Kulmala, M., Petäjä, T., Kerminen, V. M., Kujansuu, J., Ruuskanen, T., Ding, A. J., Nie, W., Hu, M., Wang, Z. B., Wu, Z. J., Wang, L., and Worsnop, D. R.: On secondary new particle formation in China, Front. Environ. Sci. Eng., 10, doi:10.1007/s11783-016-0850-1, 2016.

Li, T., Wang, Y., Li, W. J., Chen, J. M., Wang, T., and Wang, W. X.: Concentrations and solubility of trace elements in fine particles at a mountain site, southern China: regional sources and cloud processing, Atmos. Chem. Phys., 15, 8987-9002, doi:10.5194/acp-15-8987-2015, 2015a.

Li, W. J., Zhang, D. Z., Shao, L. Y., Zhou, S. Z., and Wang, W. X.: Individual particle analysis of aerosols collected under haze and non-haze conditions at a high-elevation mountain site in the North China plain, Atmos. Chem. Phys., 11, 11733-11744, doi:10.5194/acp-11-11733-2011, 2011.

Li, W. J., Chen, S. R., Xu, Y. S., Guo, X. C., Sun, Y. L., Yang, X. Y., Wang, Z. F., Zhao, X. D., Chen, J. M., and Wang, W. X.: Mixing state and sources of submicron regional background aerosols in the northern Qinghai–Tibet Plateau and the influence of biomass burning, Atmos. Chem. Phys., 15, 13365-13376, doi:10.5194/acp-15-13365-2015, 2015b.

Liu, S., Hu, M., Wu, Z., Wehner, B., Wiedensohler, A., and Cheng, Y.: Aerosol number size distribution and new particle formation at a rural/coastal site in Pearl River Delta (PRD) of China, Atmos. Environ., 42, 6275-6283, doi:10.1016/j.atmosenv.2008.01.063, 2008.

Liu, X. H., Zhu, Y. J., Zheng, M., Gao, H. W., and Yao, X. H.: Production and growth of new particles during two cruise campaigns in the marginal seas of China, Atmos. Chem. Phys., 14, 7941-7951, doi:10.5194/acp-14-7941-2014, 2014.

Manninen, H. E., Nieminen, T., Asmi, E., Gagné, S., Häkkinen, S., Lehtipalo, K., Aalto, P., Vana, M., Mirme, A., Mirme, S., Hõrrak, U., Plass-Dülmer, C., Stange, G., Kiss, G., Hoffer, A., Törő, N., Moerman, M., Henzing, B., de Leeuw, G., Brinkenberg, M., Kouvarakis, G. N., Bougiatioti, A., Mihalopoulos, N., O'Dowd, C., Ceburnis, D., Arneth, A., Svenningsson, B., Swietlicki, E., Tarozzi, L., Decesari, S., Facchini, M. C., Birmili, W., Sonntag, A., Wiedensohler, A., Boulon, J., Sellegri, K., Laj, P., Gysel, M., Bukowiecki, N., Weingartner, E., Wehrle, G., Laaksonen, A., Hamed, A., Joutsensaari, J., Petäjä, T., Kerminen, V. M., and Kulmala, M.: EUCAARI ion spectrometer measurements at 12 European sites-analysis of new particle formation events, Atmos. Chem. Phys., 10, 7907-7927, doi:10.5194/acp-10-7907-2010, 2010.

Meng, H., Zhu, Y., Evans, G. J., Jeong, C. H., and Yao, X.: Roles of SO_2 oxidation in new particle formation events, J. Environ. Sci. (China), 30, 90-101, doi:10.1016/j.jes.2014.12.002, 2015.

Mikkonen, S., Romakkaniemi, S., Smith, J. N., Korhonen, H., Petäjä, T., Plass-Duelmer, C., Boy, M., McMurry, P. H., Lehtinen, K. E. J., Joutsensaari, J., Hamed, A., Mauldin Iii, R. L., Birmili, W., Spindler, G., Arnold, F., Kulmala, M., and Laaksonen, A.: A statistical proxy for sulphuric acid concentration, Atmos. Chem. Phys., 11, 11319-11334, doi:10.5194/acp-11-11319-2011, 2011.

Qi, X. M., Ding, A. J., Nie, W., Petäjä, T., Kerminen, V. M., Herrmann, E., Xie, Y. N., Zheng, L. F., Manninen, H., Aalto, P., Sun, J. N., Xu, Z. N., Chi, X. G., Huang, X., Boy, M., Virkkula, A., Yang, X. Q., Fu, C. B., and Kulmala, M.: Aerosol size distribution and new particle formation in western Yangtze River Delta of China: two-year measurement at the SORPES station, Atmos. Chem. Phys., 15, 12491-12537, doi:10.5194/acpd-15-12491-2015, 2015.

Rose, C., Sellegri, K., Asmi, E., Hervo, M., Freney, E., Colomb, A., Junninen, H., Duplissy, J., Sipilä, M., Kontkanen, J., Lehtipalo, K., and Kulmala, M.: Major contribution of neutral clusters to new particle formation at the interface between the boundary layer and the free troposphere, Atmos. Chem. Phys., 15, 3413-3428, doi:10.5194/acp-15-3413-2015, 2015.

Saunders, R. W., Kumar, R., Martin, J. C. G., Mahajan, A. S., Murray, B. J., and Plane, J. M. C.: Studies of the Formation and Growth of Aerosol from Molecular Iodine Precursor, Z. Phys. chem., 224, 1095-1117, doi:10.1524/zpch.2010.6143, 2010.

Shen, X. J., Sun, J. Y., Zhang, X. Y., Zhang, Y. M., Zhang, L., Fan, R. X., Zhang, Z. X., Zhang, X. L., Zhou, H. G., Zhou, L. Y., Dong, F., and Shi, Q. F.: The influence of emission control on particle number size distribution and new particle

formation during China's V-Day parade in 2015, Sci. Total Environ., 573, 409-419, doi:10.1016/j.scitotenv.2016.08.085, 2016.

Sihto, S.-L., Kulmala, M., Kerminen, V.-M., Dal Maso, M., Petäjä, T., Riipinen, I., Korhonen, H., Arnold, F., Janson, R., Boy, M., Laaksonen, A., and Lehtinen, K. E. J.: Atmospheric sulphuric acid and aerosol formation implications from atmospheric measurements for nucleation and early growth mechanisms, Atmos. Chem. Phys., 6, 4079-4091, doi:10.5194/acp-6-4079-2006, 2006.

Song, M., Lee, M., Kim, J. H., Yum, S. S., Lee, G., and Kim, K.-R.: New particle formation and growth in relation to vertical mixing and chemical species during ABC-EAREX2005, Atmos. Res., 97, 359-370, doi:10.1016/j.atmosres.2010.04.013, 2010.

Sorribas, M., Adame, J. A., Olmo, F. J., Vilaplana, J. M., Gil-Ojeda, M., and Alados-Arboledas, L.: A long-term study of new particle formation in a coastal environment: meteorology, gas phase and solar radiation implications, Sci. Total Environ., 511, 723-737, doi:10.1016/j.scitotenv.2014.12.011, 2015.

Spracklen, D. V., Carslaw, K. S., Kulmala, M., Kerminen, V.-M., Sihto, S.-L., Riipinen, I., Merikanto, J., Mann, G. W., Chipperfield, M. P., Wiedensohler, A., Birmili, W., and Lihavainen, H.: Contribution of particle formation to global cloud condensation nuclei concentrations, Geophys. Res. Lett., 35, doi:10.1029/2007gl033038, 2008.

Sun, L., Xue, L. K., Wang, T., Gao, J., Ding, A. J., Cooper, O. R., Lin, M. Y., Xu, P. J., Wang, Z., Wang, X. F., Wen, L., Zhu, Y. H., Chen, T. S., Yang, L. X., Wang, Y., Chen, J. M., and Wang, W. X.: Significant increase of summertime ozone at Mount Tai in Central Eastern China, Atmos. Chem. Phys., 16, 10637-10650, doi:10.5194/acp-16-10637-2016, 2016.

Wang, D. W., Guo, H., Cheung, K., and Gan, F. X.: Observation of nucleation mode particle burst and new particle formation events at an urban site in Hong Kong, Atmos. Environ., 99, 196-205, doi:10.1016/j.atmosenv.2014.09.074, 2014a.

Wang, H., Zhu, B., Shen, L., An, J., Yin, Y., and Kang, H.: Number size distribution of aerosols at Mt. Huang and Nanjing in the Yangtze River Delta, China: Effects of air masses and characteristics of new particle formation, Atmos. Res., 150, 42-56, doi:10.1016/j.atmosres.2014.07.020, 2014b.

Wang, Z. B., Hu, M., Yue, D. L., Zheng, J., Zhang, R. Y., Wiedensohler, A., Wu, Z. J., Nieminen, T., and Boy, M.: Evaluation on the role of sulfuric acid in the mechanisms of new particle formation for Beijing case, Atmos. Chem. Phys., 11, 12663-12671, doi:10.5194/acp-11-12663-2011, 2011.

Wang, Z. B., Hu, M., Pei, X. Y., Zhang, R. Y., Paasonen, P., Zheng, J., Yue, D. L., Wu, Z. J., Boy, M., and Wiedensohler, A.: Connection of organics to atmospheric new particle formation and growth at an urban site of Beijing, Atmos. Environ., 103, 7-17, doi:10.1016/j.atmosenv.2014.11.069, 2015.

Wehner, B., Wiedensohler, A., Tuch, T. M., Wu, Z. J., Hu, M., Slanina, J., and Kiang, C. S.: Variability of the aerosol number size distribution in Beijing, China: New particle formation, dust storms, and high continental background, Geophys. Res. Lett., 31, doi:10.1029/2004gl021596, 2004.

Xiao, S., Wang, M. Y., Yao, L., Kulmala, M., Zhou, B., Yang, X., Chen, J. M., Wang, D. F., Fu, Q. Y., Worsnop, D. R., and Wang, L.: Strong atmospheric new particle formation in winter in urban Shanghai, China, Atmos. Chem. Phys., 15, 1769-1781, doi:10.5194/acp-15-1769-2015, 2015.

Young, L. H., Benson, D. R., Montanaro, W. M., Lee, S. H., Pan, L. L., Rogers, D. C., Jensen, J., Stith, J. L., Davis, C. A., Campos, T. L., Bowman, K. P., Cooper, W. A., and Lait, L. R.: Enhanced new particle formation observed in the northern midlatitude tropopause region, J. Geophys. Res.- Atmos., 112, D10218, doi:10.1029/2006JD008109, 2007.

Yue, D. L., Hu, M., Wang, Z. B., Wen, M. T., Guo, S., Zhong, L. J., Wiedensohler, A., and Zhang, Y. H.: Comparison of particle number size distributions and new particle formation between the urban and rural sites in the PRD region, China, Atmos. Environ., 76, 181-188, doi:10.1016/j.atmosenv.2012.11.018, 2013.

Zhang, R.: Getting to the Critical Nucleus of Aerosol Formation, Science, 328, 1366-1367, 2010.

Zhang, R., Khalizov, A., Wang, L., Hu, M., and Xu, W.: Nucleation and growth of nanoparticles in the atmosphere, Chem. Rev., 112, 1957-2011, doi:10.1021/cr2001756, 2012.

Zhang, X., Yin, Y., Lin, Z., Han, Y., Hao, J., Yuan, L., Chen, K., Chen, J., Kong, S., Shan, Y., Xiao, H., and Tan, W.: Observation of aerosol number size distribution and new particle formation at a mountainous site in Southeast China, Sci. Total Environ., 575, 309-320, doi:10.1016/j.scitotenv.2016.09.212, 2016.

Zhang, X. H., Zhang, Y. M., Sun, J. Y., Zheng, X. J., Li, G., and Deng, Z. Q.: Characterization of particle number size

distribution and new particle formation in an urban environment in Lanzhou, China, J. Aerosol Sci., 103, 53-66, doi:10.1016/j.jaerosci.2016.10.010, 2017.

Zhang, Y. M., Zhang, X. Y., Sun, J. Y., Lin, W. L., Gong, S. L., Shen, X. J., and Yang, S.: Characterization of new particle and secondary aerosol formation during summertime in Beijing, China, Tellus B, 63, 382-394, doi:10.1111/j.1600-0889.2011.00533.x, 2011.

Zhang, Y. M., Zhang, X. Y., Sun, J. Y., Hu, G. Y., Shen, X. J., Wang, Y. Q., Wang, T. T., Wang, D. Z., and Zhao, Y.: Chemical composition and mass size distribution of PM1 at an elevated site in central east China, Atmos. Chem. Phys., 14, 12237-12249, doi:10.5194/acp-14-12237-2014, 2014.

Zhu, Y., Sabaliauskas, K., Liu, X., Meng, H., Gao, H., Jeong, C.-H., Evans, G. J., and Yao, X.: Comparative analysis of new particle formation events in less and severely polluted urban atmosphere, Atmos. Environ., 98, 655-664, doi:10.1016/j.atmosenv.2014.09.043, 2014.

Figure and Table captions

Fig. 1. Average diurnal variations of the condensation sink, sulfuric acid proxy, trace gases (SO_2 and O_3), and meteorological conditions (T and RH) during NPF days and non-NPF days over all the campaigns at the summit of Mt. Tai.

Fig. 2. The relationships between the sulfuric acid proxy, condensation sink and particle number concentration of 3-6 nm ($N_{3\text{-}6}$) in the early morning (6:00-9:00 LT) on NPF days (a) and non-NPF days (b). The data are hourly averages, and the spot color represents the values of $N_{3\text{-}6}$ (cm^{-3}).

Fig. 3. The particle number concentration of 3-6 nm ($N_{3\text{-}6}$, blue) and sulfuric acid concentration ($[H_2SO_4]$, red) on 14 October 2014, fitting a good correlation (R^2 =0.975) during NPF event (6:00-14:00 LT).

Fig. 4. Time series during 10 November-9 December 2014 and the shaded areas are NPF days: (a) contour plot of the particle number size distributions using NAIS data; (b) sulfur dioxide (blue) and ozone (red); (c) meteorological parameters, including wind speed (cyan), wind direction (green), temperature (magenta) and relative humidity (earth yellow).

Fig. 5. Wind rose plots of all the NPF days (a) and non-NPF days (b), and the wind speed and wind direction between 07:00 and 11:00 LT are included. Length of each spoke on the circle represents the probability of wind coming from a particular direction at the certain range of wind speed.

Fig. 6. Air mass back trajectories for 72 h at 6:00 LT at 1535 m ASL on all the NPF days (a) and non-NPF days (b)

Fig. 7. Time series of the particle size distributions, meteorological parameters, trace gases, chemical composition and mass concentration of $PM_{2.5}$ on 11 November 2014.

Fig. 8. Air mass backward trajectories for 72 h at 1535 m ASL at 6:00 (A), 8:00 (B), 10:00 (C), 12:00 (D) and 14:00 LT (E) on 11 November 2014.

Table 1. The calculated parameters of all the NPF events during three campaigns, the minimums and maximums are marked in blue and red, respectively.

Table 2. Summary of the mean, median, 25th percentile, 75th percentile, minimum and maximum for the calculated parameters on the basis of the Table 1

Table 3. The NPF characteristics comparison between Mt. Tai and other typical researches in China

Table 4. The parameters on four NPF hazy days and the averages of all the NPF days during daytime (6:00-18:00 LT)

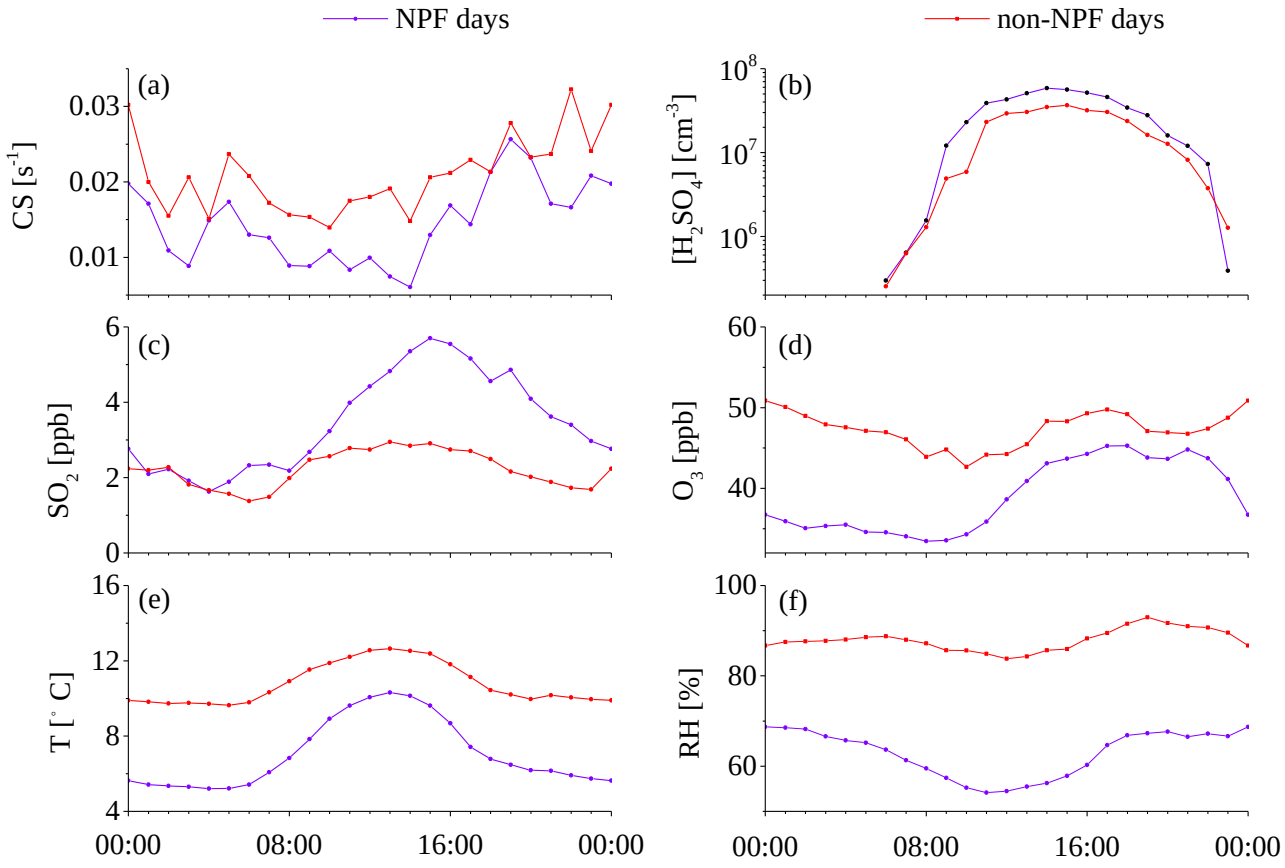

Fig. 1. Average diurnal variations of the condensation sink, sulfuric acid proxy, trace gases (SO_2 and O_3), and meteorological conditions (T and RH) during NPF days and non-NPF days over all the campaigns at the summit of Mt. Tai.

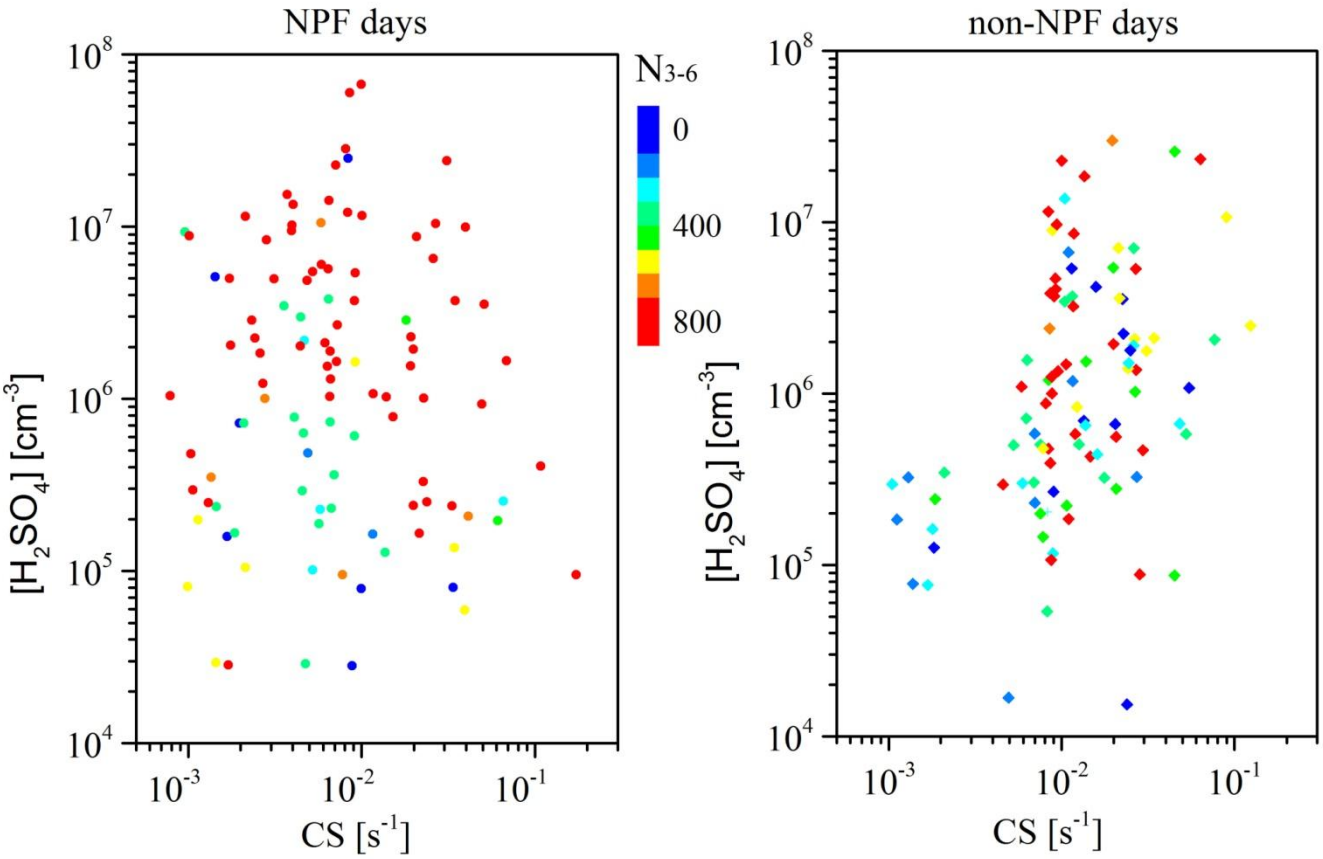

Fig. 2. The relationships between the sulfuric acid proxy, condensation sink and particle number concentration of 3-6 nm ($N_{3\text{-}6}$) in the early morning (6:00-9:00 LT) on NPF days (a) and non-NPF days (b). The data are hourly averages, and the spot color represents the values of $N_{3\text{-}6}$ (cm^{-3}).

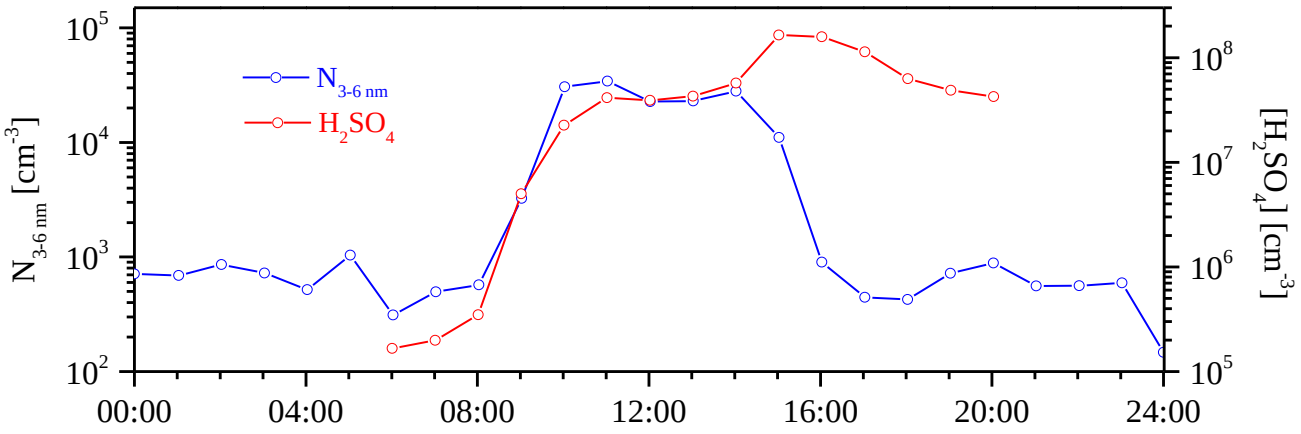

Fig. 3. The particle number concentration of 3-6 nm ($N_{3\text{-}6}$, blue) and sulfuric acid proxy concentration ([H_2SO_4], red) on 14 October 2014, fitting a good correlation (R^2 =0.975) during NPF event (6:00-14:00 LT).

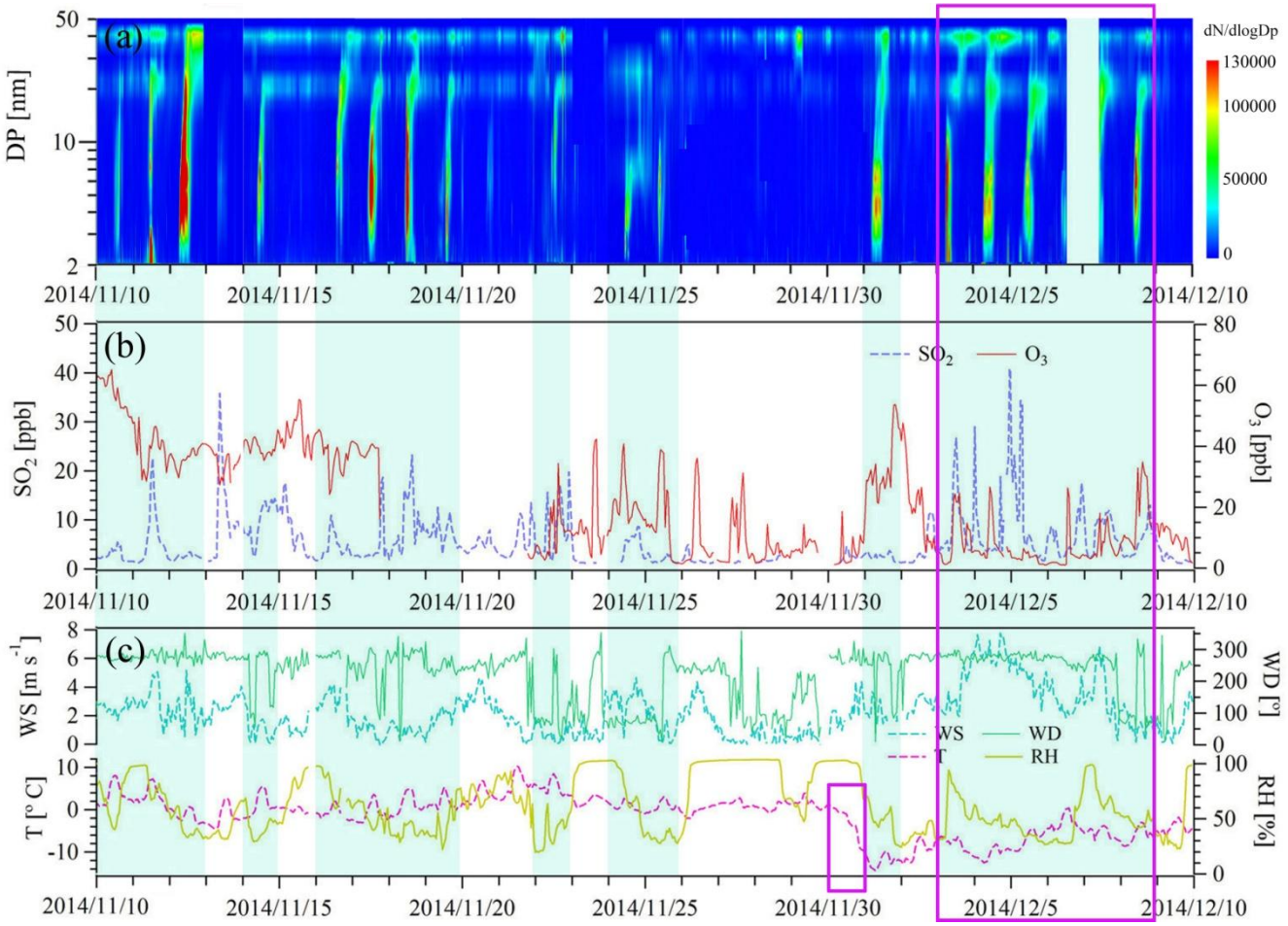

Fig. 4. Time series during 10 November-9 December 2014 and the shaded areas are NPF days: (a) contour plot of the particle number size distributions using NAIS data; (b) sulfur dioxide (blue) and ozone (red); (c) meteorological parameters, including wind speed (cyan), wind direction (green), temperature (magenta) and relative humidity (earth yellow)

5

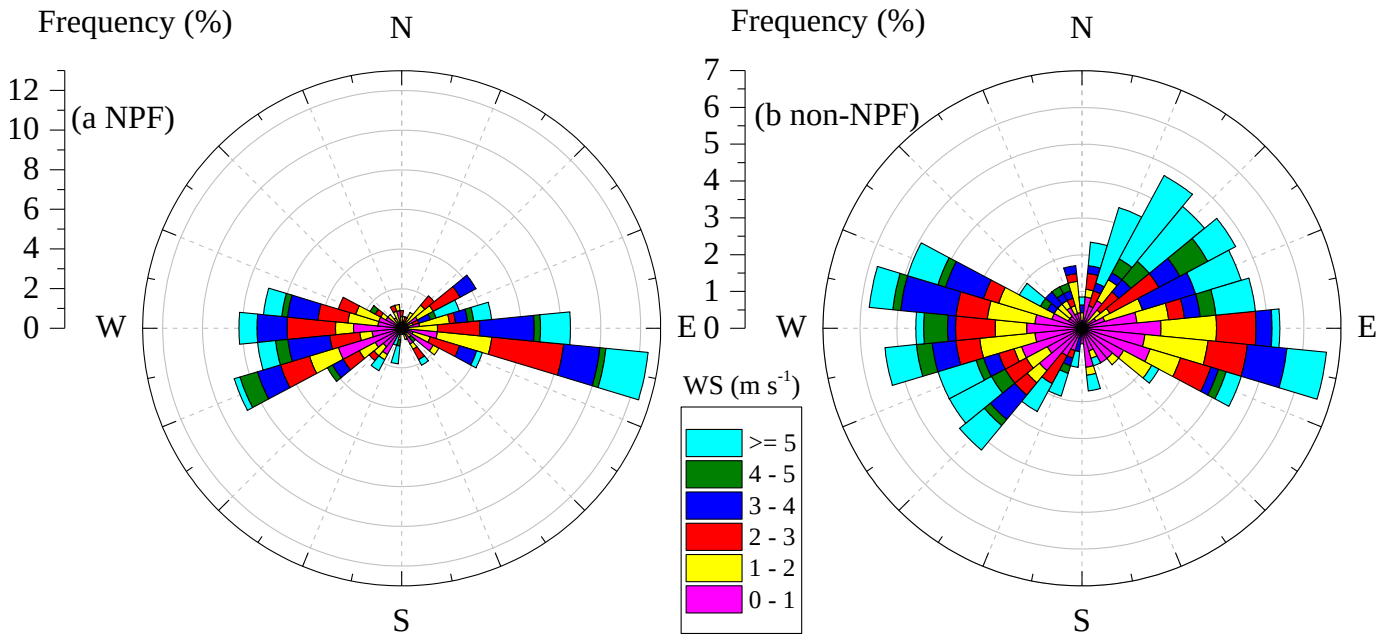

Fig. 5. Wind rose plots of all the NPF days (a) and non-NPF days (b), and the wind speed and wind direction between 07:00 and 11:00 LT are included. Length of each spoke on the circle represents the probability of wind coming from a particular direction at the certain range of wind speed.

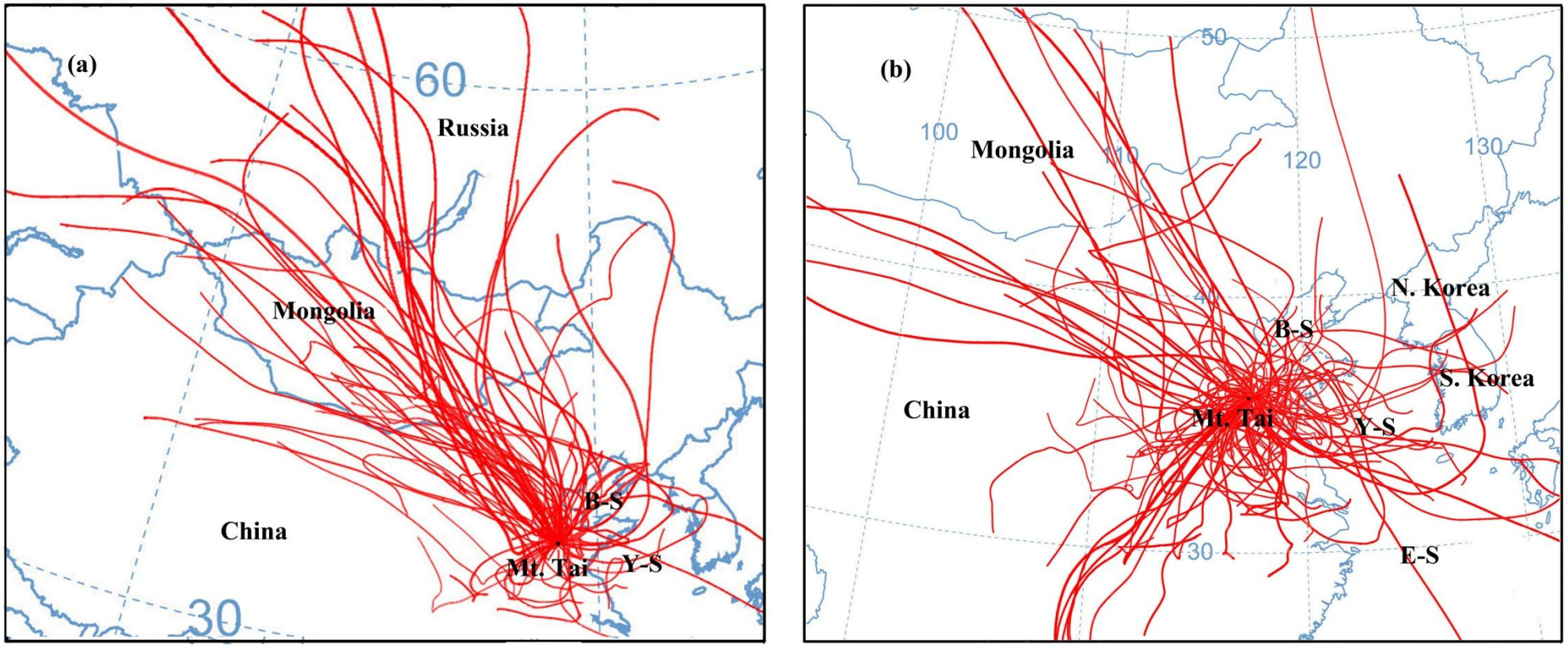

Fig. 6. Air mass back trajectories for 72 h at 6:00 LT at 1535 m ASL on all the NPF days (a) and non-NPF days (b)

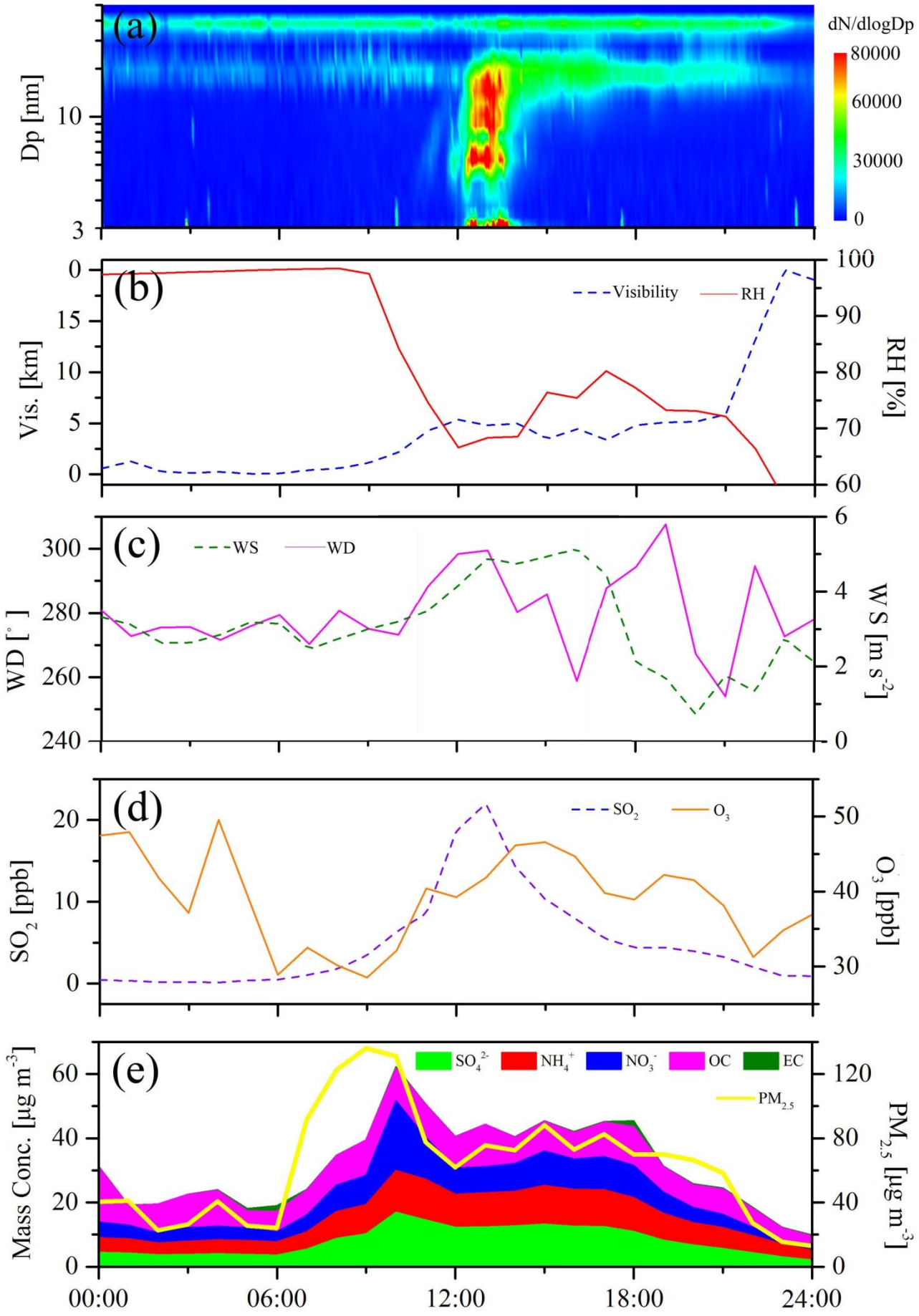

Fig. 7. Time series of the particle size distribution, meteorological parameters, trace gases, chemical composition and mass concentration of $PM_{2.5}$ on 11 November 2014.

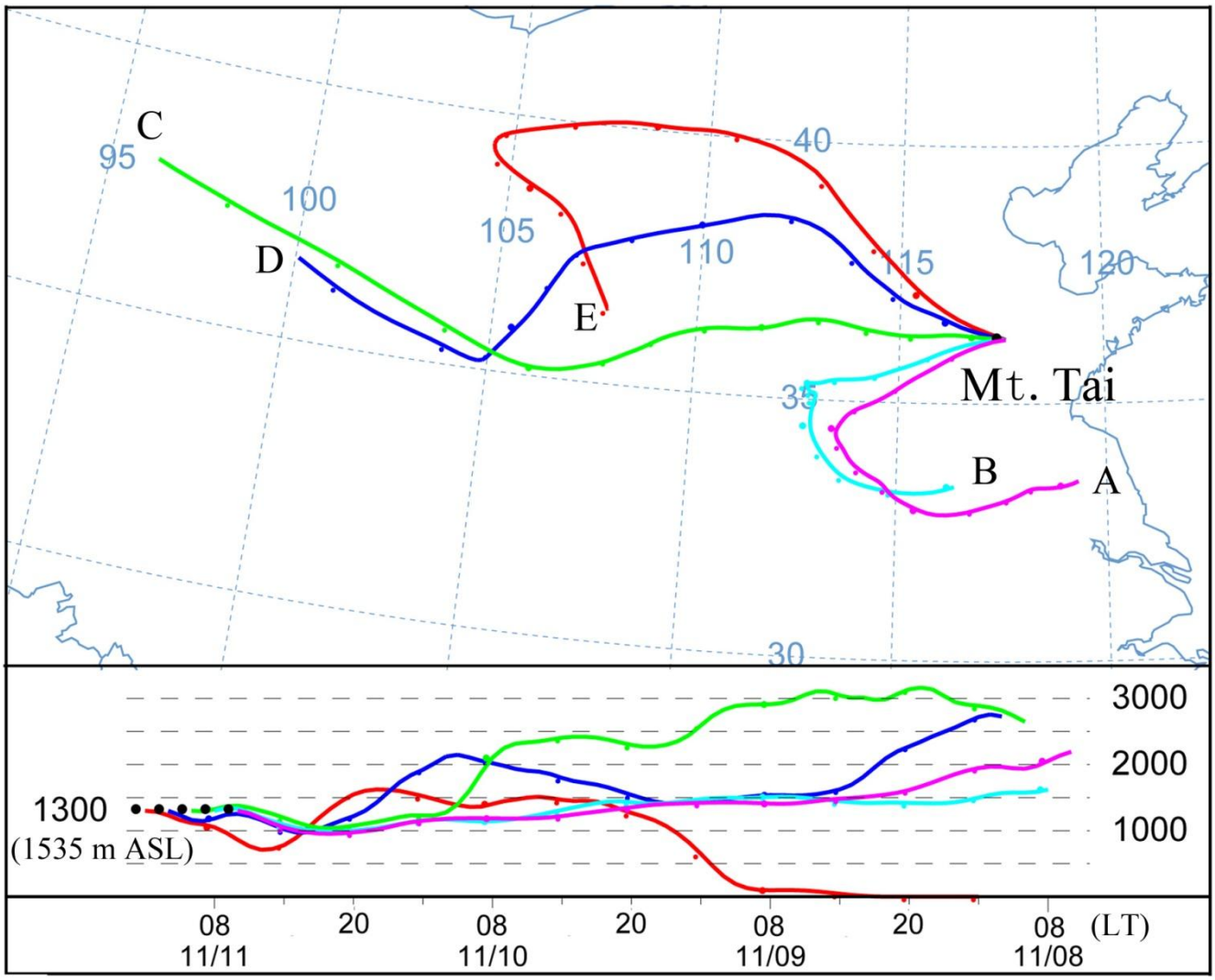

Fig. 8. Air mass backward trajectories for 72 h at 1535 m ASL at 6:00 (A), 8:00 (B), 10:00 (C), 12:00 (D) and 14:00 LT (E) on 11 November 2014.

Table 1. The calculated parameters of all the NPF events during three campaigns, the minimums and maximums are marked in blue and red, respectively.

Campaign	Date	J_3 cm^{-3} s^{-1}	J_{3-20} cm^{-3} s^{-1}	GR $nm\ h^{-1}$	CS 10^{-2} s^{-1}	$[H_2SO_4]$ 10^6 cm^{-3}	SO_2 ppb	O_3 ppb	Date	J_3 cm^{-3} s^{-1}	J_{3-20} cm^{-3} s^{-1}	GR $nm\ h^{-1}$	CS 10^{-2} s^{-1}	$[H_2SO_4]$ 10^6 cm^{-3}	SO_2 ppb	O_3 ppb
I	26-Jul-14	3.34	13.32	1.54	0.5-3.1	N/A	N/A	56±7	8-Aug-14	2.61	16.30	1.15	1.8-15.9	2.87	2.7±2.3	65±10
	27-Jul-14	0.94	6.12	1.55	0.6-2.1	N/A	2.4±2.0	56±9	11-Aug-1	N/A	1.44	1.71	0.2-6.9	3.81	0.6±0.5	56±6
	2-Aug-14	N/A	3.60	3.81	0.1-8.7	N/A	N/A	22±13	12-Aug-1	N/A	40.13	3.69	0.8-7.4	22.1	10.8±7.9	79±16
	3-Aug-14	N/A	1.69	**7.76**	0.1-26.9	N/A	1.5±1.2	35±17	15-Aug-1	2.75	4.52	3.00	N/A	N/A	1.0±1.0	63±12
	6-Aug-14	23.90	52.54	5.78	0.2-1.9	N/A	4.8±2.6	50±5	20-Aug-1	**0.82**	1.33	4.80	0.6-2.7	9.25	5.2±4.3	72±8
	7-Aug-14	N/A	10.90	1.45	0.1-24.8	N/A	1.5±1.7	56±4								
II	22-Sep-14	0.99	1.58	1.12	0.7-9.0	7.74	5.7±1.7	76±8	4-Nov-14	7.73	15.06	0.77	0.6-1.5	5.39	6.3±1.2	56±3
	29-Sep-14	16.63	54.97	1.13	0.7-21.1	2.43	1.4±1.1	48±5	6-Nov-14	0.98	**1.10**	1.45	0.1-1.2	2.02	0.6±0.5	13±5
	30-Sep-14	7.94	20.61	1.62	0.5-28.4	1.09	1.9±0.5	2±1	7-Nov-14	1.40	5.59	1.26	0.1-2.0	0.93	0.4±0.3	23±11
	2-Oct-14	5.16	12.02	1.15	0.2-6.6	1.98	1.6±1.7	41±4	8-Nov-14	9.40	13.53	2.95	0.4-2.3	6.71	4.1±2.6	38±3
	3-Oct-14	5.44	14.07	1.50	0.1-4.6	1.34	0.7±0.7	42±3	10-Nov-1	1.02	2.17	3.41	N/A	N/A	2.3±0.7	60±4
	5-Oct-14	8.13	26.41	2.00	0.5-6.9	**0.52**	0.2±0.1	11±5	11-Nov-1	3.29	14.42	2.52	N/A	N/A	7.8±8.3	34±5
	6-Oct-14	2.54	8.94	0.78	0.4-3.4	0.53	0.3±0.4	7±2	12-Nov-1	12.39	26.36	1.09	N/A	N/A	1.6±0.4	35±2
	8-Oct-14	N/A	1.40	0.92	N/A	N/A	5.0±0.6	71±6	14-Nov-1	9.92	13.41	1.55	N/A	N/A	6.1±4.0	40±2
	10-Oct-14	6.54	27.04	1.80	0.2-1.6	4.33	1.8±2.1	54±3	16-Nov-1	5.36	11.06	2.47	0.5-1.2	11.6	5.7±2.9	34±6
	11-Oct-14	9.43	20.37	0.70	0.2-2.2	1.50	3.1±2.5	68±6	17-Nov-1	9.15	16.82	1.10	0.2-0.9	8.38	1.5±0.2	38±2
	13-Oct-14	6.17	26.84	1.64	0.4-2.0	7.43	5.1±1.6	27±8	18-Nov-1	20.45	57.11	0.80	0.1-1.6	4.42	N/A	N/A
	14-Oct-14	10.15	18.11	1.55	0.1-1.4	1.43	0.9±0.8	44±4	19-Nov-1	8.89	15.41	2.51	0.3-2.8	N/A	N/A	N/A
	15-Oct-14	6.76	30.54	2.76	N/A	N/A	10.1±2.9	60±6	22-Nov-1	N/A	11.60	1.23	0.3-5.6	4.18	5.3±4.9	10±8
	16-Oct-14	6.14	36.96	**0.58**	N/A	N/A	1.5±1.9	41±1	24-Nov-1	11.03	24.51	1.50	N/A	N/A	2.9±2.1	26±10
	17-Oct-14	1.55	5.75	2.12	N/A	N/A	N/A	N/A	25-Nov-1	7.11	10.97	2.02	0.1-2.9	N/A	0.5±0.4	25±13
	18-Oct-14	6.16	22.89	2.03	N/A	N/A	N/A	N/A	1-Dec-14	4.96	7.55	1.77	0.1-0.9	1.22	1.4±0.3	27±4
	21-Oct-14	N/A	1.98	2.36	0.4-1.3	N/A	0.3±0.3	13±5	3-Dec-14	**25.04**	**57.43**	1.51	0.4-1.4	1.64	12.9±9.6	13±11
	24-Oct-14	3.64	8.99	1.25	0.5-1.3	1.12	N/A	N/A	4-Dec-14	4.80	10.62	2.69	0.4-1.4	5.48	2.9±0.3	13±9
	25-Oct-14	7.50	14.74	1.60	0.4-1.4	0.89	0.3±0.3	15±11	5-Dec-14	3.34	5.83	1.32	0.2-1.2	0.95	N/A	4±1
	27-Oct-14	7.24	15.49	0.99	N/A	N/A	0.2±0.3	12±4	6-Dec-14	N/A	1.52	1.99	N/A	N/A	2.2±1.2	4±9
	28-Oct-14	2.98	13.17	1.21	N/A	N/A	0.2±0.1	5±2	7-Dec-14	N/A	11.64	1.42	N/A	N/A	7.9±2.5	8±5
	2-Nov-14	11.24	17.78	0.72	0.2-0.9	4.97	0.7±0.1	33±3	8-Dec-14	9.78	16.33	1.24	N/A	N/A	2.4±1.4	16±10
	3-Nov-14	8.77	18.57	1.10	0.3-1.3	6.65	4.6±0.6	37±3								
III	16-Jun-15	1.45	9.22	3.98	1.7-4.9	13.6	6.3±0.8	105±7	4-Jul-15	12.55	23.25	0.91	N/A	N/A	5.7±2.9	95±20
	20-Jun-15	6.16	32.50	3.28	0.5-1.8	10.5	2.8±1.6	81±11	8-Jul-15	N/A	8.25	0.93	0.6-2.3	N/A	0.5±0.5	90±16
	21-Jun-15	3.90	6.08	3.44	1.4-3.0	**25.7**	10.0±2.1	105±15	13-Jul-15	N/A	5.64	1.95	1.0-2.4	1.10	0.1±0.1	110±15
	2-Jul-15	9.61	43.41	1.08	0.2-1.9	N/A	2.2±1.3	69±10	15-Jul-15	N/A	19.72	2.86	0.7-1.6	N/A	0.2±0.1	88±12
	3-Jul-15	5.54	10.86	2.65	0.2-2.1	N/A	5.5±2.5	101±13	25-Jul-15	N/A	19.56	1.88	0.4-1.9	2.41	0.3±0.2	99±9

Table 2. Summary of the mean, median, 25th percentile, 75th percentile, minimum, and maximum for the calculated parameters on the basis of the Table 1

	Mean	Minimum	Maximum	25th percentile	Median	75th percentile
J_3 (cm^{-3} s^{-1})	7.10	0.82	25.04	3.31	6.15	9.41
$J_{3\text{-}20}$ (cm^{-3} s^{-1})	16.61	1.10	57.43	6.12	13.47	20.61
GR (nm h^{-1})	1.98	0.58	7.76	1.15	1.55	2.51
CS (10^{-2} s^{-1})	1.4	0.1	28.4	0.5	0.9	1.7
[H_2SO_4] (10^6 cm^{-3})	5.23	0.52	25.7	1.28	3.34	7.07
SO_2 (ppb)	3.2	0.1	12.9	0.7	2.2	2.7
O_3 (ppb)	45	2	110	19	41	66

Table 3. The NPF characteristics comparison between Mt. Tai and other typical researches in China

Observation site	FR (cm^{-3} s^{-1})	GR (nm h^{-1})	Freq.	Data	Air mass style	Ref.
Mt. Tai	7.10±5.39 (J_3)	1.98±1.27 (GR_{3-20})	40 %	Jul-Dec 2014 & Jun-Aug 2015	Mountain (1534 m ASL)	This study
Mt. Tai Mo Shan	0.97-10.2 ($J_{5.5}$)	1.5-8.4 ($GR_{5.5-25}$)	33 %	Oct-Nov 2010	Mountain (640 m ASL)	Guo et al. (2012)
Mt. Huang	0.09-0.30 (J_{10})	1.42-4.53 (GR_{10-20})	37 %	Apr-Jul 2008	Mountain (1840 m ASL)	Zhang et al. (2016)
Mt. Huang		2.29-4.27 (GR_{10-15})	18 %	Sep-Oct 2012	Mountain (869 m ASL)	Hao et al. (2015)
Mt. Daban		0.8-3.2	79 %	Sep-Oct 2013	Mountain (3295 m ASL)	Du et al. (2015)
SouthYellow Sea & East China Sea	0.3-15.2 ($J_{5.6-30}$)	2.5-5.0	16 %	Oct-Nov 2011 & Nov 2012	Marine	Liu et al. (2014)
Backgarden	2.4-4.0 (J_{3-25})	4.0-22.7 (GR_{3-25})	25 %	Jul 2006	Rural	Yue et al. (2013)
Nanjing	2.6 (J_6)	10.4 (GR_{6-30})	44 %	Dec 2011-Nov 2013	Suburban	Qi et al. (2015)
Lanzhou		1.2-16.9 (GR_{10-20})	33 %	Jun-Jul 2006	Suburban	Gao et al. (2012)
Xinken	0.5-5.2 (J_{3-20})	2.2-19.8 (GR_{3-20})	26 %	Oct-Nov 2004	Suburban	Liu et al. (2008)
Shanghai	2.3-19.2 (J_3)	1.9-38.3 (GR_{7-20})	21 %	Nov 2013-Jan 2014	Urban	Xiao et al. (2015)
Nanjing	1.6-6.7 (J_{10-25})	5.6-9.6 (GR_{10-25})	40 %	Jul-Aug 2012	Urban	An et al. (2015)
Beijing	5.0-44.9 (J_3)	1.86-6.7 (GR_{7-30})	26 %	Jul-Sep 2008	Urban	Wang et al. (2015)
Lanzhou	0.2-6.2 ($J_{14.6-25}$)	2.6-12.3 ($GR_{14.6-25}$)	34 %	Aug-Nov 2014	Urban	Zhang et al. (2017)
Qingdao	13.3 ($J_{5.6-30}$)	2.0-10.2	41 %	Apr-May 2010	Urban	Zhu et al. (2014)
Hong Kong	1.9 ($J_{5.5}$)	3.7-8.3 ($GR_{5.5-10}$)	23 %	Dec 2010-Jan 2011	Urban	Wang et al. (2014a)

Table 4. The parameters on four NPF hazy days and the averages of all the NPF days during daytime (6:00-18:00 LT)

	T (℃)	RH (%)	WS ($m\ s^{-1}$)	SO_2 (ppb)	O_3 (ppb)	NO_2 (ppb)	CO (ppb)	$PM_{2.5}$ ($\mu g\ m^{-3}$)
Averages	5.4	54	2.1	3.9	31	10.5	759	31
26-Jul-14	19.6±2.1	67±10	0.7±0.4	5.4±3.4	65±12	N/A	N/A	42±3
17-Oct-14	12.8±2.6	59±11	2.7±0.4	N/A	N/A	10.0±4.2	827±256	121±97
18-Oct-14	14.0±2.0	55±8	1.5±0.4	N/A	N/A	7.1±1.9	757±40	49±18
11-Nov-14	4.8±1.9	82±12	3.7±1.1	8.1±6.7	38±6	11.9±3.1	1641±284	84±30